Ab initio molecular-dynamics method based on the restricted path integral: Application to the electron plasma and liquid alkali metal

Ki-dong Oh
Department of Physics, University of Arizona, Tucson, Arizona 85721

P. A. Deymier
Department of Materials Science and Engineering, University of Arizona, Tucson, Arizona 85721
(Received 29 April 1998)

We introduce an *ab initio* molecular-dynamics method based on the discretized path-integral representation of quantum particles. Fermi statistics is automatically generated by an effective exchange potential. This path-integral molecular-dynamics method is able to simulate electron plasmas at the border of the degenerate and the semidegenerate regimes with a satisfactory level of accuracy. Application of the method to the simulation of a liquid alkali metal demonstrates its potential in the simulation of real systems from first principles. [S0163-1829(98)00436-6]

I. INTRODUCTION

Modeling and simulation have become a vital part of materials research. Modeling and simulation techniques are maturing to the point where they offer hope for a practical and reliable approach for the study of real materials. The development of materials models has evolved from the infancy of specific empirical descriptions to highly accurate and sophisticated representations based on first-principle calculations. *Ab initio* molecular-dynamics (MD) methods relying on density-functional theory (DFT) within the local-density approximation[1,2] are emerging as some of the most powerful tools for investigating the properties of complex many-body systems. These methods have enjoyed a great popularity and have been employed to investigate a very large number of problems.[3] In contrast to the DFT MD method, molecular-dynamics simulations using the discretized path-integral[4] representation of quantum particles have been limited mostly to the simulation of systems containing a small number of quantum degrees of freedom such as in the solvation of a single quantum particle in a classical fluid[5] or to problems where quantum exchange is not dominant.[6] We should also mention the path-integral-based method of Alavi and Frenkel that allows for the calculation of the grand canonical partition function of fermion systems.[7] With this method the fermion sign problem in the evaluation of the partition function is solved exactly in the case of noninteracting fermions. When combined with DFT, this method provides a means of doing *ab initio* MD of systems with interacting high-temperature electrons.[8]

Progress in the simulation of fermionic systems by the path-integral Monte Carlo method[9–12] has opened the way to the implementation of a path-integral-based finite-temperature *ab initio* molecular-dynamics (PIMD) method. This paper describes such a molecular-dynamics method applicable to the simulation of many-fermion systems at finite temperatures. The method is based on (a) the discretized path-integral representation of quantum particles as closed ''polymeric'' chains of classical particles (beads) coupled through harmonic springs,[4] (b) the treatment of quantum exchange as cross linking of the chains,[13] (c) the nonlocality of cross linking (exchange) along the chains (in imaginary time),[9] and (d) the restricted path integral[10,14] to resolve the problem of negative weights to the partition function resulting from the cross linking of even numbers of quantum particles.

The present PIMD method is initially applied to the description of the one-component plasma (OCP) at the border of the degenerate and semidegenerate regimes where the ratio of the temperature to the Fermi temperature T_F is approximately equal to 0.1. The electron plasma is the first focus of this investigation because it is the simplest electronic system. It has been extensively studied via path-integral, variational, and diffusion Monte Carlo methods since the calculation of the equation of states of a Fermi OCP such as the interacting electron gas is a problem of fundamental and practical importance as one uses its properties in density-functional theory. The OCP is also a good prototypical system as there exists a large amount of theoretical and numerical data on its equation of state. The zero-temperature perturbative expansion of the energy of a three-dimensional uniform electron plasma in the high-density limit (when r_s, the radius of a sphere that encloses on the average one particle, is much smaller than the Bohr radius a_0) was calculated theoretically quite some time ago.[15] Accurate Monte Carlo variational calculations have extended the $T=0$ K equation of states of the degenerate Fermi OCP to a wide range of lower densities $r_s/a_0 \in [1,500]$.[16] The exchange-correlation free energy has been subsequently calculated to encompass the full range of thermal degeneracy.[17–19]

After showing that the PIMD method contains the necessary ingredients to simulate electron plasmas up to metal densities at finite temperatures, we turn to demonstrating that it is applicable to simulating a liquid metal from first principle. We focus on a simple alkali metal, namely, liquid K. We chose potassium because (i) it is a prototypical free-electron metal, (ii) there exist experimental data for the pair-correlation function,[20] and (iii) the DFT MD method has had problems with metals when electrons leave the Born-Oppenheimer surface and therefore violate one of the basic

assumption of the method. This problem has been solved technically in an *ad hoc* manner with the introduction of appropriate thermostats for the electronic and ionic degrees of freedom.[21] In our model, the discretized restricted path-integral representation of the electron is the same as that of the electron plasma. Classical ionic degrees of freedom representing potassium ions are added to the model. The electrons are interacting with the ions via a simple empty core local pseudopotential. We show that bonding takes place and that the calculated structure of the liquid is in good agreement with experimental data.

The present paper is organized as follows. We introduce the PIMD method in Sec. II. Features specific to the simulation of the models of the electron plasma and liquid alkali metal along with results are reported in Sec. III. Conclusions regarding the effectiveness of the PIMD model are drawn in Sec. IV along with future improvements.

II. METHOD

The partition function of a system of N quantum particles expressed in a position representation may take the form[22]

$$Z=\int dR_1\rho(R_1,R_1;\beta), \tag{1}$$

where ρ is the density matrix, $R_1=\{\mathbf{r}^{(1)},\ldots,\mathbf{r}^{(N)}\}$ stands for position of the particles, and $\beta=1/kT$. Using the convolution property of the density matrix

$$\rho(R_1,R_3;\beta_1+\beta_2)=\int dR_2\rho(R_1,R_2;\beta_1)\rho(R_2,R_3;\beta_2) \tag{2}$$

and introducting P-1 intermediate states, Z is written in a discretized path-integral representation

$$Z=\int \prod_{n=1}^{P} dR_n \prod_{n=1}^{P}{}^{*}\rho(R_n,R_{n+1};\epsilon), \tag{3}$$

where $\epsilon=\beta/P$ and the asterisk in the product indicates the cyclic condition $R_{P+1}=R_1$.

Since the wave function of fermions (electrons) is antisymmetric, the density matrix can be positive or negative and convergence of the summation may be slow. However, the diagonal density matrix can be evaluated by restricting paths to remain in the region of phase space where their sign is positive.[10] It is therefore possible to write

$$Z=\int \prod_{n=1}^{P} dR_n \prod_{n=1}^{P}{}^{*}\rho(R_n,R_{n+1};\epsilon)\,\theta^{+}. \tag{4}$$

The parameter θ^{+} is equal to 1 for positive paths and 0 otherwise. The quantum partition function can now be cast in the form of a classical partition function

$$Z=\int \prod_{n=1}^{P} dR_n \exp[-\beta V_{\mathrm{eff}}(R_1,\ldots,R_P)], \tag{5}$$

with

$$V_{\mathrm{eff}}=\begin{cases} -\dfrac{1}{\beta}\displaystyle\sum_{n=1}^{P}{}^{*}\ \ln\rho(R_n,R_{n+1},\epsilon) & \text{if } \theta^{+}=1 \\ \infty & \text{if } \theta^{+}=0. \end{cases} \tag{6}$$

The classical form of Eq. (5) suggests that a molecular-dynamics scheme could be used to sample the states of the quantum system. A microcanonical ensemble sampling of the states of the system can now be performed by solving for the trajectories generated by the classical Hamiltonian

$$H=\sum_{i=1}^{N}\sum_{n=1}^{P}\tfrac{1}{2}m^{*}(\dot{r}_n^{(i)})^2+V_{\mathrm{eff}}(R_1,\ldots,R_P;\epsilon). \tag{7}$$

Here m^{*} is some arbitrary mass used to define an artificial kinetic energy for the quantum states in order to explore the potential surface V_{eff}. Since the effective potential presents an infinite potential barrier to paths attempting to change sign, the molecular-dynamics scheme offers the advantage of automatically imposing the restriction on the density matrix to the region of phase space where the paths are positive.

Equation (4) is exact, but since one does not know the exact density matrix, it is necessary to replace it by some reasonable approximation. The nodes (loci of points where the density matrix is zero) of the approximate density matrix should be as close as possible to those of the exact density matrix if one hopes to calculate accurate properties of a fermion system.

The exact density matrix is approximated by a nonlocal form of the noninteracting density matrix. In the limit of high temperature, the nodes of the noninteracting density matrix approximate reasonably well those of the exact density matrix.[10] If P is sufficiently large, we can use Trotter's approximation to separate the kinetic and the potential contributions to the density matrix.[23]

The propagator $\rho(R_n,R_{n+1};\epsilon)$ is approximated for small ϵ, using the Trotter formula,[23] by

$$\begin{aligned}\rho(R_n,R_{n+1};\epsilon)&=\langle R_n|\exp(-\epsilon H_{\mathrm{op}})|R_{n+1}\rangle \\ &\approx\int dR\langle R_n|\exp(-\epsilon T_{\mathrm{op}})|R\rangle \\ &\quad\times\langle R|\exp(-\epsilon V_{\mathrm{op}})|R_{n+1}\rangle,\end{aligned} \tag{8}$$

where the Hamiltonian operator H_{op} is decomposed into the kinetic operator T_{op} and the potential operator V_{op}. For a local potential operator ρ becomes

$$\rho(R_n,R_{n+1};\epsilon)\approx\langle R_n|\exp(-\epsilon T_{\mathrm{op}})|R_{n+1}\rangle\exp[-\epsilon V(R_{n+1})], \tag{9}$$

where $V(R_{n+1})$ is a potential function of the position. This potential function may describe any potential field in which the electrons evolve including electron-electron Coulomb interactions or electron-ion interactions.

For the kinetic matrix we use the exact noninteracting density matrix

$$\langle R_n|\exp(-\epsilon T_{\mathrm{op}})|R_{n+1}\rangle=\left[\frac{m}{2\pi\epsilon\hbar^2}\right]^{3N/2}\det[A_{n,n+1}], \tag{10}$$

with $[A_{n,n+1}]$ representing an $N\times N$ matrix whose elements are expressed as

$$A^{ij}_{n,n+1}=\exp\left[-\beta\,\frac{m}{2\beta\epsilon\hbar^2}\,(r^{(i)}_n-r^{(j)}_{n+1})^2\right]. \tag{11}$$

Up to this point the density matrix has been projected on a Slater determinant of plane waves and is equivalent to a Hartree-Fock approximation.

The determinant of the kinetic matrix in the absence of quantum exchange is factored out of Eq. (10):

$$\det[A_{n,n+1}]=\prod_{i=1}^{N} A^{ii}_{n,n+1}\,\det[E_{n,n+1}], \tag{12}$$

where all the exchange effects (including the sign of the density matrix) are included in $[E]$. In the absence of exchange the matrix $[E]$ reduces to the identity matrix. The elements of $[E]$ are defined as $E^{ij}_{n,n+1}=A^{ij}_{n,n+1}/A^{ij}_{n,n+1}$. In the limit of $\epsilon\rightarrow 0$, the matrix $[E]$ converges to the identity matrix and the system collapses into a bosonic state. To prevent this undesirable behavior, following Hall,[9] we recast Eq. (12) in a nonlocal form

$$\det[A_{n,n+1}]=\prod_{i=1}^{N} A^{ii}_{n,n+1}\prod_{m=1}^{P}\,(\det[E_{n,m}])^{1/P}. \tag{13}$$

This nonlocal form is equivalent to a mean-field approximation over all possible exchange processes. In this form the density matrix does not correspond anymore to a projection over a single Slater determinant of plane waves and therefore may represent the quantum system beyond a Hartree-Fock model.

With the restricted path integral, the integrand of the partition function is positive and Z can now be rewritten in a classical form usable with a molecular-dynamics scheme:

$$Z=\int\prod_{n=1}^{P} dR_n\exp[-\beta V^{\rm exch}_{\rm eff}(R_1,\ldots,R_P)], \tag{14}$$

where the effective potential includes quantum exchange. In the case of a nonpolarized fermion system with $N_{\rm el}$ electrons, a microcanonical ensemble sampling of the quantum states of the system can now be performed by solving for the trajectories generated by a classical Hamiltonian of the type given in Eq. (7). The time trajectories thus obtained do not have real meaning but are only a mean to explore the effective exchange potential surface:

$$\begin{aligned}V^{\rm exch}_{\rm eff}(R_1,\ldots,R_P)=&\sum_{i=1}^{P}\sum_{k>l}^{N_{\rm el}}\sum_{l=1}^{N_{\rm el}-1}\frac{(-e)(-e/P)}{4\pi\epsilon_0|r^{(k)}_i-r^{(l)}_i|}\\&+\sum_{k=1}^{N_{\rm el}}\sum_{i=1}^{P}{}^{*}\,\frac{m_eP}{2\hbar^2\beta^2}\,(r^{(k)}_i-r^{(k)}_{i+1})^2\\&-\frac{1}{\beta}\sum_{s=\uparrow}^{\downarrow}\frac{\sum_{i=1}^{P}\sum_{j=1}^{P}\ln\det[E_{ij}]_s\theta^+_{ijs}}{\sum_{i=1}^{P}\sum_{j=1}^{P}\theta^+_{ijs}}.\end{aligned} \tag{15}$$

The third term in Eq. (15) is an effective exchange potential for the electrons with spin up ($s=\uparrow$) and spin down ($s=\downarrow$). The function θ^+_{ij} ensures the path restriction by taking on the values 1 and 0 for paths with positive and negative $\det[E]$, respectively. The first term of this Hamiltonian accounts for the electron/electron Coulomb interactions.

Extension of the restricted PIMD method to include classical ionic degrees of freedom is straightforward provided the electrons interact with the ions via local pseudopotentials. In this case the Hamiltonian becomes

$$\begin{aligned}H=&\sum_{k=1}^{N_{\rm el}}\sum_{i=1}^{P}\frac{1}{2}\,m^*(\dot r^{(k)}_i)^2+\sum_{I=1}^{N_{\rm ion}}\frac{1}{2}\,M_I\dot R_I^2\\&+\sum_{I>J}^{N_{\rm ion}}\sum_{I=1}^{N_{\rm ion}-1}\Phi_{IJ}(r_{IJ})+\sum_{i=1}^{P}\sum_{k>1}^{N_{\rm el}}\sum_{l=1}^{N_{\rm el}-1}\frac{(-e)(-e/P)}{4\pi\epsilon_0|r^{(k)}_i-r^{(l)}_i|}\\&+\sum_{i=1}^{P}\sum_{k=1}^{N_{\rm el}}\sum_{I=1}^{N_{\rm ion}}\frac{V_{\rm pseudo}(R_I-r^{(k)}_i)}{P}\\&+\sum_{k=1}^{N_{\rm el}}\sum_{i=1}^{P}{}^{*}\,\frac{m_eP}{2\hbar^2\beta^2}\,(r^{(k)}_i-r^{(k)}_{i+1})^2\\&-\frac{1}{\beta}\sum_{s=\uparrow}^{\downarrow}\frac{\sum_{i=1}^{P}\sum_{j=1}^{P}\ln\det[E_{ij}]_s\theta^+_{ijs}}{\sum_{i=1}^{P}\sum_{j=1}^{P}\theta^+_{ijs}}.\end{aligned} \tag{16}$$

The differences between the Hamiltonians (7) and (16) include a kinetic energy for the ionic degrees of freedom as well as the ion/ion Φ_{IJ} and ion/electron $V_{\rm pseudo}$ interaction potentials.

III. MODEL SYSTEMS AND RESULTS

A. Electron plasma

We have tested the PIMD method on an unpolarized electron plasma composed of $N_{\rm el}=30$ electrons ($N_\uparrow=15$ and $N_\downarrow=15$). The simulation cell is a fixed cubic box with edge lengths $L=13.3$, 19.95, and 26.6 Å, which correspond to electronic densities with $r_s/a_0=5$, 7.5, and 10, respectively. Periodic boundary conditions are used and the system is constituted of a simulation cell and 26 image cells. Under these conditions the matrix $[E_{n,m}]$ for each spin should be a $27N_{\uparrow,\downarrow}\times 27N_{\uparrow,\downarrow}$ matrix. In order to make the calculation more tractable, we make the numerical approximation $\det[E_{n,m}]\approx C\,\det[F_{n,m}]$, where $[F_{n,m}]$ is an $N_{\uparrow,\downarrow}\times N_{\uparrow,\downarrow}$ matrix that off-diagonal elements give the maximum contribution of pair exchange to the determinant among the possible combinations of exchange between the electrons in the simulation cell and the electrons in all periodic cells. $C\approx\overline{\det[F]}^{26}$ is a constant representing the mean contribution of the image cells to the overall determinant. Within this approximation, the constant C drops out of the force calculation. This approximation should be valid at high temperature when the electrons are fairly well localized and for systems in which the electrons have a strong repulsive interaction that prevents the close approach of more than a very few electrons at a time. In this form, the computing time for the calculation of

the exchange potential scales as $P^2N_{\uparrow,\downarrow}^3$. This scaling at present limits the applicability of the method to systems with a fairly small number of fermions. However, one may exploit the natural parallelism of the approximate effective exchange potential over the number of beads to reduce the computational cost to a nearly linear scaling with respect to P.[24]

We solve the equation of motion with a leapfrog scheme and an integration time step of $\sim 10^{-16}$ sec. Most simulations were run for an average of 30 000 time steps. In some cases for the low and intermediate density plasmas, we have run simulations up to 50 000 steps for better equilibration, at low temperature.

Because of the large computational cost of the calculation of the exchange effective potential and forces, the exchange forces are calculated and updated every ten MD time steps. The values for the exchange forces are used subsequently during the ten steps following their calculation. We have compared the calculated average energies during a simulation where the exchange forces were calculated every step and the more efficient scheme described above and found no significant statistical difference in their values.

The chosen time step is small enough to resolve the high-frequency oscillations of the harmonic springs. In the case of systems with large P, the strong harmonic forces in Eq. (15) may lead to nonergodic behaviors.[25] This problem can be alleviated by rescaling temperature with a chain of Nosé-Hoover thermostats.[6,26] This rescaling would ensure convergence to the right canonical distribution. We have elected to rescale the temperature of each chain of P beads independently of each other via a simple momentum rescaling thermostat.[27] With this procedure we do not obtain a true canonical distribution, but most thermal averages will be accurate to orders N^{-1}.[28] We have also verified that with this approach over the length of our simulations the chains would sample a large region of configuration space and therefore resolve not only the fast but also the slow dynamical scale.

The calculation of the Coulomb energy is handled by the usual Ewald method of summation.[29] The Coulomb potential energy of the electron plasma is made convergent by the introduction of a positively charged background of density $-30e/\Omega$, where Ω is the cell volume. The discretized nature of the quantum particle introduces some peculiarity in the calculation of the Coulomb potential. The potential at a bead n of an electron i is therefore given by[16]

$$u_{i,n}=\frac{1}{4\pi\epsilon_0}\frac{(-e)}{P}\left\{\sum_{\substack{j\neq i\\ \text{if } j \text{ in cell}}}^{N_{\rm el}}\frac{1}{r_{ij,n}}\,\mathrm{erfc}(\eta r_{ij,n})-2\frac{\eta}{\sqrt{\pi}}\right.$$
$$+\sum_{k\neq 0}^{\infty}\frac{4\pi}{\Omega}\frac{e^{-k^2/4\eta^2}}{k^2}\sum_{\substack{j=1\\ j \text{ in cell}}}^{N_{\rm el}}e^{i\mathbf{k}\cdot(\mathbf{r}_{j,n}-\mathbf{r}_{i,n})}$$
$$\left.-\frac{\pi(N_{\rm el}-1)}{\Omega\eta^2}\right\}, \qquad (17)$$

where k is a reciprocal space vector associated with the periodicity of the simulated and image systems. erfc stands for the complementary error function. The first three terms in Eq. (17) are the usual real and reciprocal space contributions to the potential. The last term is the contribution of the background. We chose an Ewald parameter $\eta=5.741/L$ for which satisfactory convergence is obtained with truncation of the real space sum at $\frac{1}{2}L$ and truncation of the reciprocal sum at $k^2\leqslant 49$.

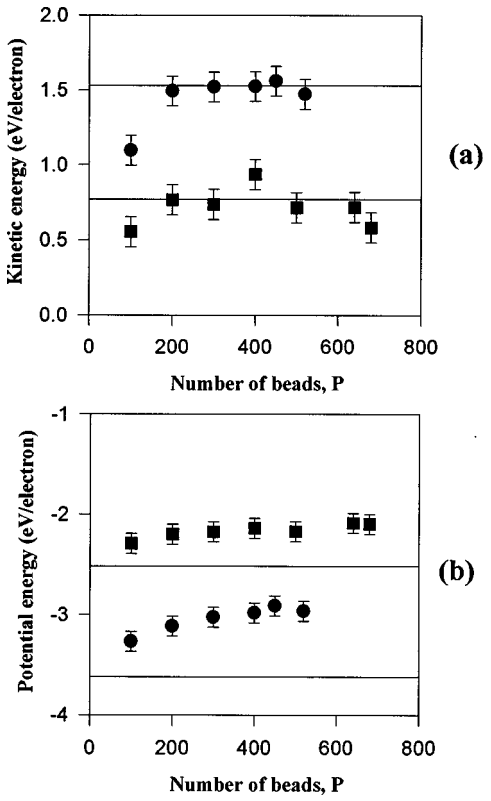

FIG. 1. (a) Kinetic energy and (b) potential energy as functions of the number of beads in the necklace representation of quantum particles. The circles and squares refer to the high-density ($r_s=5a_0$, $T=1800$ K) and medium-density ($r_s=7.5a_0$, $T=700$ K) electron plasmas, respectively.

We calculate the kinetic energy with the usual energy estimator derived from $\partial \ln Z/\partial\beta$.[5] Hall has shown that the exchange potential does not contribute directly to the actual energy estimator but indirectly through the equilibrium configurations.[9] With this estimator, the kinetic energy is given as a small quantity, the difference between two larger quantities, with a variance growing with P. This estimator therefore introduces an error on the calculated values of the kinetic energy that we have estimated to be on the order of 0.1 eV.

Every simulation reported starts with a different initial configuration obtained from randomly generated bead position in every electron chain. The initial bead-bead distance is determined by the temperature. In order to reduce the time for the system to reach equilibrium from its initial configuration, we have taken some care as to construct initial configurations closely related to the anticipated equilibrium state. Specifically, we have found that localized compact necklaces take more time to reach equilibrium compared to more open necklaces whose beads are distributed uniformly throughout the simulation cell. This observation is more important for low-density systems where the extent of space to sample is large.

In Fig. 1 we present results on the convergence of the discretized restricted path-integral molecular dynamics. The

kinetic energy [Fig. 1(a)] and potential energy [Fig. 1(b)] of the high-density plasma ($r_s=5a_0$) at $T=1800$ K and the intermediate-density plasma ($r_s=7.5a_0$) at a temperature of 700 K are reported as a function of the number of beads P. We note that the energies converge to some asymptotic value for necklaces containing as few as 200–300 beads even for the electron plasma near metallic density. This observation is particularly significant as the nonparallelized PIMD algorithm scales with the square of the number of beads. In addition to PIMD energies, we have also indicated the 0-K kinetic and potential energies of electron plasma with same density of Ref. 16. At the temperatures of 1800 and 700 K, the high- and intermediate-density systems are in the degenerate regime and the electronic energies should be comparable to the 0-K values. The kinetic energies are in very good agreement, but some discrepencies exist between the potential energies as the restricted PIMD method appears to overestimate them. In order to further the validation of the restricted PIMD method, we have conducted a series of calculations at several temperatures for the three densities. For the high- and medium-density systems we have used 450 and 300 beads, respectively. These numbers of beads fall within the region of convergence. Electrons in the low-density electron plasma are discretized over 360, 380, 450, 680, 720, and 780 beads for the temperatures 1100, 900, 650, 575, and 550; 500 and 450; and 400 and 350 K. The calculated kinetic energies of Fig. 2(a) are in excellent agreement with the variational Monte Carlo results of Ceperley[16] for correlated plasma. We note that the kinetic energy does not vary significantly over the range of temperature studied, as is expected for these plasmas at the border of the degenerate and the semidegenerate regimes.[18] At low temperature, the low-density system with a large number of beads takes a very long time to equilibrate and sampling of phase space is not very efficient. In this case, calculation of reliable energies requires very long simulations. Another difficulty in calculating reliable energies when a large number of beads are used results from the fact, as was noted before, that the variance of the kinetic energy increases with P. We did not need to use so many nodes for the low-density plasma even at low temperature; however, these simulations illustrate the need to use as few beads as possible within the interval of convergence. In addition to the 0-K correlated energies, we have indicated the Hartree kinetic energy ($2.21/r_s^2$ in rydbergs) with a dotted line. Figure 2(a) shows that the nonlocal form of the density matrix given by Eq. (13) introduces some electron correlation. This is also apparent in the results for the temperature dependence of the potential energy. The calculated potential energy falls between the fully correlated results of Ceperley and the electron/electron interaction contribution to the Hartree-Fock energy (given by $-0.916/r_s$ in rydbergs). We also note that the potential energy increases weakly with temperature and that extrapolation toward 0 K should result in potential energies in better agreement with the correlated potential energies than the uncorrelated ones. In the present model, however, the nonlocal effective potential introduces an electron correlation between electrons with identical spins only. The present potential energies are overestimated as correlations between electrons with opposite spins are not accounted for.

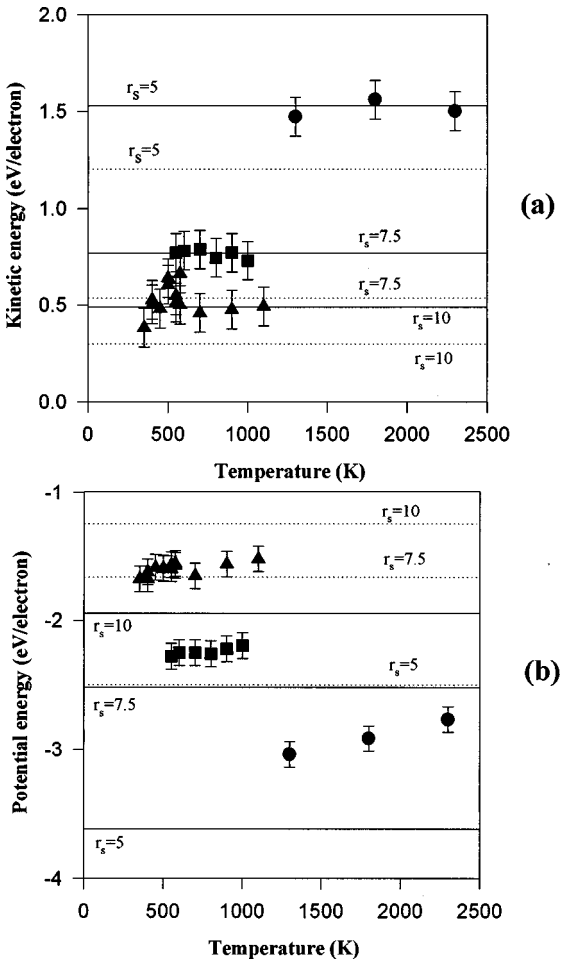

FIG. 2. (a) Kinetic energy and (b) potential energy as functions of temperature. The electron plasmas with $r_s=5a_0$, $7.5a_0$, and $10a_0$ are denoted by circles, squares, and triangles, respectively. The horizontal lines correspond to the correlated energies of Ceperley (Ref. 16). The dotted lines indicate the Hartree-Fock energies.

Finally, as a demonstration of the effectiveness of the exchange potential in Eq. (15), the pair correlation for isospin and heterospin electrons is reported in Fig. 3 in the case of the high-density plasma at the three temperatures studied. The difference between iso- and heterospin radial distributions is striking. In order to satisfy Pauli exclusion principle, the nonlocal exchange potential keeps the electrons with identical spin away from each other while electrons with different spins can approach each other quite closely. The Coulomb repulsive force is the only force keeping electrons with different spins from approaching. The nonlocal exchange potential is quite short range as it does not appear to affect the electron distribution beyond 5 Å. The exclusion is particularly important in the interval]0,3 Å]. The major effect of a rising temperature is the increase in pair correlation at shorter distance or, in other words, the shrinkage of the exchange-correlation hole.[18] After showing that the nonlocal restricted PIMD method can simulate with reasonable accuracy electron plasma near metal density, we apply the method to the simulation of an alkali metal from first principles.

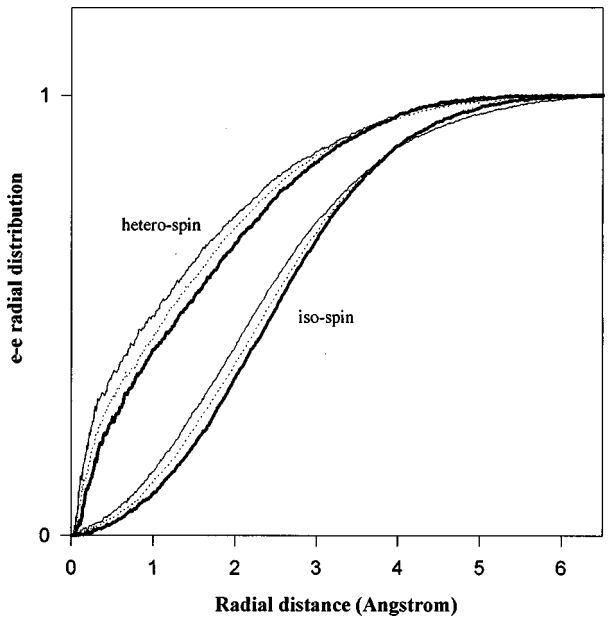

FIG. 3. Isospin and heterospin electron-electron pair distributions for the high-density electron plasma at $T=1300$ K (thick solid line), $T=1800$ K (dotted line), and $T=2300$ K (thin solid line).

B. Alkali metal

The alkali-metal system is composed of 30 K^+ ions and 30 electrons in a cubic box with dimension $L=13.3$ Å. The electron density in this system gives $r_s=5a_0$. The electrons are nonpolarized. The Hamiltonian describing the system is given by Eq. (16). The numerical treatment of the electrons is done in a fashion similar to that of the electron plasmas. In the model, the K^+ ions are dealt with in a purely classical manner and interact through a Born-Mayer potential

$$\Phi_{IJ}(r)=\frac{Z_I Z_J e^2}{4\pi\epsilon_0 r}+A_{IJ}e^{-r/\rho_{IJ}} \tag{18}$$

and the parameters of the potential are those fixed by Sangster and Atwood.[30] As to the electron/ion interaction, we have used a simple empty core local pseudopotential

$$V_{\text{pseudo}}(r)=\begin{cases}\dfrac{-Z_I e^2}{r}, & r\geqslant R_c\\ \dfrac{-Z_I e^2}{R_c}, & r<R_c,\end{cases} \tag{19}$$

with a core radius $R_c=2.22$ Å.[31]

To optimize the calculation, we do not use the Ewald summation but simply replace the long-range Coulomb potential in Eqs. (18) and (19) by a shorter-range effective potential of the form

$$\frac{1}{r}\rightarrow\frac{1}{r}\,\text{erfc}(\eta r), \tag{20}$$

where $\eta=5.741/L$. The shorter-range potential is then truncated at half the size of the edge of the simulation box.

The melting point of potassium is $T_m=337$ K. The simulation of liquid potassium near this temperature would necessitate a large number of beads for convergence of the electronic degrees of freedom with respect to P. We have seen that in the study of the electron plasma at high density ($r_s=5a_0$), the electron system conserves a nearly degenerate character up to a temperature of 2300 K. Since temperature does not affect significantly the electronic states at the metal density, we have decoupled thermally the classical ionic degrees of freedom and the quantum electronic degrees of freedom. The electronic necklaces are attached to a thermostat set at a temperature of 1300 K while the ion temperature is adjusted independently with another thermostat. At the electron temperature of 1300 K, a number of beads $P=360$ is sufficient for convergence of the discretized path.

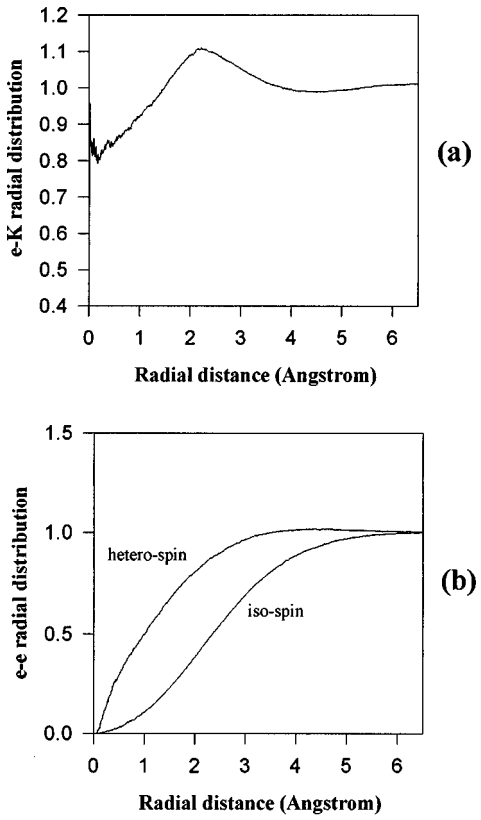

FIG. 4. (a) Electron-potassium and (b) electron-electron pair distributions for liquid K at $T=337$ K.

The physical potassium ion mass is $M_I=71\,830m_e$, leading to an extreme disparity in electronic and ionic time scales. For practical reasons, we use a ratio of the ion mass M_I to the electron bead artificial mass m^* of 39.1:1. The dynamics of the electrons is still significantly faster than the dynamics of the ions. The MD integration time step is the same as for the electron plasma. The ion and electron positions in the initial configurations are generated at random with the electron necklace bead/bead distance constrained by the temperature. We have run two simulations lasting 50 000 MD integration steps. In the first simulation the ions and electrons thermostats are both set at the temperature of 1300 K. The ion temperature is maintained at 337 K for the second simulation.

The electronic structure of the liquid alkali metal is best illustrated by the electron-ion and electron-electron radial distributions. These distributions are reported for liquid potassium near the melting point. Figure 4(a) shows that the electrons are concentrating on the periphery of the ion core. The electrons participate in bonding as indicated by the fact that they are not localized within the core of each ion. In Fig.

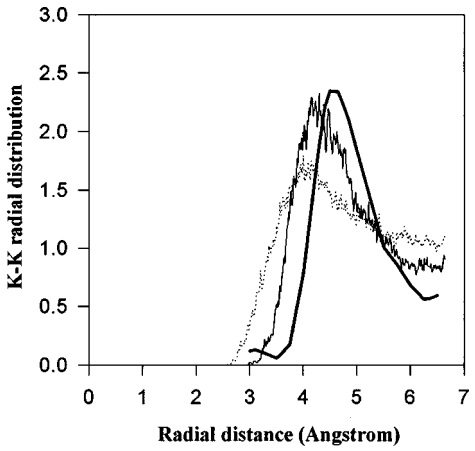

FIG. 5. Calculated ion-ion pair distribution function at $T = 337$ K (thin solid line) and 1300 K (dotted line) and the experimentally measured distribution (Ref. 20, thick solid line).

4(b) we have plotted the electron-electron radial distribution for iso- and heterospin electrons. These distributions are similar to those of the high-density electron plasma. This behavior is therefore characteristic of a free-electron–like material. An increase in temperature of the ions to 1300 K does not affect significantly the electron-electron and electron-ion pair distributions.

Figure 5 shows the K-K radial distribution at the two temperatures studied compared to the experimental measurement.[20] As was expected, the prominent peak is softened as the temperature increases since the ions have larger displacements at higher temperatures. Very similar results have been found in DFT MD calculations of the structure of liquid sodium.[32] The calculated pair distribution is in reasonable agreement with the experimental data, although the nearest-neighbor distance is underestimated by approximately 0.3 Å. The reasons for this deviation are threefold. First, the electron-ion pseudopotential we have used is quite approximate and may be improved upon. Second, as seen in the simulation of the electron plasma, heterospin electron correlations are not included in the model. Finally, the simulated alkali liquid system contains only a very small number of ions, which may lead to a size effect. The effect of the small size of the system is particularly large at radial distances in the range 6–7 Å, which corresponds to the cutoff of the electrostatic potential.

IV. CONCLUSIONS

We have shown that a nonlocal form of the restricted discretized path integral may be used to define an effective exchange potential for use in molecular-dynamics simulations of quantum particles obeying Fermi statistics. A quantum particle is represented as a closed necklace of discrete beads. Exchange is described via nonlocal cross linking of the necklaces. We have demonstrated that electron plasmas may be simulated with a satisfactory degree of accuracy with this method up to metallic densities. The algorithm converges rather quickly with respect to the number of beads, rendering it practical computationally. We have noted that the exchange potential appears to introduce correlation in some effective form. Correlation would only be accounted for for isospin electrons, which may explain the overestimated potential energy. A solution to that problem may be to employ a fully correlated density matrix.[33]

We have extended the restricted PIMD method to include the electron-ion interaction via a simple pseudopotential and therefore allowing in the future the simulation of materials from first principles. We have simulated liquid potassium near the melting point and compared the calculated structure to an experimentally determined pair correlation function. In view of the approximate pseudopotential we have used as well as the small size of the simulation cell, remarkable agreement is achieved. At present, however, the restricted PIMD method is limited by the computation cost of the forces derived from the effective exchange potential. Access to supercomputers can make possible the simulation of larger systems. For larger fermion systems, one may be able to optimize the calculation by exploiting the short spatial extent of exchange[34] and dividing the simulation cell into smaller and more tractable subcells. Since the PIMD method involves stiff oscillators, disparate masses, and short- and long-range forces, another avenue to improve the computational efficiency of our algorithm is to employ a multiple time step scheme.[35–37]

Because of its computational limitations the restricted PIMD method introduced herein may be particularly suited to investigating materials with low electron densities $\sim 10^{21}$ cm^{-3} where quantum exchange is still important. This is the case, for instance, in doped or nonstoichiometric ceramic oxides where the bonding between the ionic degrees of freedom may be modeled classically through semiempirical potentials and the remaining few electronic degrees of freedom by discretized quantum paths.[38]

[1] R. Car and M. Parrinello, Phys. Rev. Lett. **55**, 2471 (1985).
[2] A. Selloni, P. Carnevali, R. Car, and M. Parrinello, Phys. Rev. Lett. **59**, 823 (1987).
[3] M. Parrinello, Solid State Commun. **102**, 107 (1997).
[4] R. P. Feynman and A. R. Hibbs, *Quantum Mechanics and Path Integrals* (McGraw-Hill, New York, 1965).
[5] M. Parrinello and A. Rahman, J. Chem. Phys. **80**, 860 (1984).
[6] D. Marx and M. Parrinello, Z. Phys. B **95**, 143 (1994).
[7] A. Alavi and D. Frenkel, J. Chem. Phys. **97**, 9249 (1992).
[8] A. Alavi, J. Kohanoff, M. Parrinello, and D. Frenkel, Phys. Rev. Lett. **73**, 2599 (1994).
[9] R. W. Hall, J. Chem. Phys. **89**, 4212 (1988); **93**, 5628 (1989); **91**, 1926 (1989).
[10] D. M. Ceperley, Phys. Rev. Lett. **69**, 331 (1992).
[11] D. M. Ceperley, Rev. Mod. Phys. **67**, 279 (1995).
[12] S. Zhang, J. Carlson, and J. E. Gubernatis, Phys. Rev. B **55**, 7464 (1997).
[13] D. Chandler and P. G. Wolynes, J. Chem. Phys. **74**, 4078 (1981).
[14] D. M. Ceperley, J. Stat. Phys. **63**, 1237 (1991).
[15] M. Gell-Mann and K. Bruekner, Phys. Rev. **106**, 364 (1957).
[16] D. M. Ceperley, Phys. Rev. B **18**, 3126 (1978); D. M. Ceperley and B. J. Alder, Phys. Rev. Lett. **45**, 566 (1980).

[17] F. Perrot and M. W. C. Dharma-wardana, Phys. Rev. A **30**, 2619 (1984).
[18] R. G. Dandrea, N. W. Ashcroft, and A. E. Carlsson, Phys. Rev. B **34**, 2097 (1986).
[19] S. Tanaka, S. Mitake, and S. Ichimaru, Phys. Rev. A **32**, 1896 (1985).
[20] Y. Waseda, in *The Structure of Non-Crystalline Materials* (McGraw-Hill, New York, 1980).
[21] P. E. Blochl and M. Parrinello, Phys. Rev. B **45**, 9413 (1992).
[22] R. P. Feynman, *Statistical Mechanics* (Benjamin, New York, 1972).
[23] H. Kleinert, *Path Integral Quantum Mechanics, Statistics, and Polymer Physics* (World Scientific, Singapore, 1990).
[24] Ki-dong Oh and P. A. Deymier (unpublished).
[25] R. W. Hall and B. J. Berne, J. Chem. Phys. **81**, 3641 (1984).
[26] G. J. Martyna, M. L. Klein, and M. Tuckerman, J. Chem. Phys. **97**, 2635 (1992).
[27] L. V. Woodcock, Chem. Phys. Lett. **10**, 257 (1971).
[28] M. J. Gillan, in *Computer Modelling of Fluids, Polymers and Solids*, edited by C. R. A. Catlow *et al.* (Kluwer Academic, Dordrecht, 1990), p. 155.
[29] C. Kittel, *Introduction to Solid State Physics*, 6th ed. (Wiley, New York, 1986).
[30] M. J. L. Sangster and R. M. Atwood, J. Phys. C **11**, 1541 (1978).
[31] W. A. Harrison, *Pseudopotentials in the Theory of Metals* (Benjamin, New York, 1966).
[32] G.-X Qian, M. Weinert, G. W. Fernando, and J. W. Davenport, Phys. Rev. Lett. **64**, 1146 (1990).
[33] G. Senger, M. L. Ristig, C. E. Campbell, and J. W. Clark, Ann. Phys. (N.Y.) **218**, 160 (1992).
[34] X. P. Li, R. W. Numes, and D. Vanderbilt, Phys. Rev. B **47**, 10 891 (1993).
[35] M. E. Tuckerman, B. J. Berne, and A. Rossi, J. Chem. Phys. **94**, 1465 (1991).
[36] M. E. Tuckerman, B. J. Berne, and G. J. Martyna, J. Chem. Phys. **97**, 1990 (1992).
[37] D. A. Gibson and E. A. Carter, J. Phys. Chem. **97**, 13429 (1993).
[38] C. Y. Lee and P. A. Deymier, Solid State Commun. **102**, 653 (1997).